Nuclear Instruments and Methods in Physics Research A 763 (2014) 260–265

Contents lists available at ScienceDirect

Nuclear Instruments and Methods in Physics Research A

journal homepage: www.elsevier.com/locate/nima

Scalable large-area solid-state neutron detector with continuous p–n junction and extremely low leakage current

Kuan-Chih Huang [a], Rajendra Dahal [a,b], James J.-Q. Lu [a], Adam Weltz [b], Yaron Danon [b,*], Ishwara B. Bhat [a,*]

[a] Department of Electrical, Computer, and Systems Engineering, Rensselaer Polytechnic Institute, Troy, NY 12180-3522, USA
[b] Department of Mechanical, Aerospace, and Nuclear Engineering, Rensselaer Polytechnic Institute, Troy, NY 12180-3522, USA

ARTICLE INFO

Article history:
Received 7 January 2014
Received in revised form
26 April 2014
Accepted 12 June 2014
Available online 21 June 2014

Keywords:
Solid-state neutron detector
Large area
Continuous p–n junction
Low leakage current
Neutron detection efficiency

ABSTRACT

We report on the fabrication and characterization of solid-state thermal neutron detectors with detection areas up to 16 cm^2 that require only a single preamplifier for data acquisition. These detectors consist of a honeycomb-like micro-structured Si diode with boron-10 filled deep holes. A continuous p–n junction formed over the entire surface of the microstructure helps to achieve a low leakage current density of $\sim 6.1 \times 10^{-9}$ A/cm^2 at -1 V for a 2.5×2.5 mm^2 detector. This low leakage current results in low electronic noise, which enables the fabrication of large-area detectors. An intrinsic thermal neutron detection efficiency of up to 26% was measured for a 2.5×2.5 mm^2 detector module and up to 24% was measured for a 1 cm^2 detector module. These measurements were obtained under zero bias voltage using a moderated californium-252 source. The relative efficiency remains almost the same when scaling the detector area up to 8 cm^2 by connecting 1 cm^2 detector modules in series. However, it decreases to 0.89 and 0.82, respectively, for 12 and 16 cm^2. Nevertheless, these results demonstrate the promise of using boron filled micro-structured Si diodes as a cost effective alternative to the helium-3 based neutron detection technology and the potential of fabricating scalable large-area solid-state neutron detectors that are desirable for many applications.

1. Introduction

Neutron detectors are useful for a variety of applications including homeland security, nuclear safeguards and process monitoring [1]. For these applications, detectors with low bias voltages can be advantageous. Additionally, both compact detectors and large detection area detectors are desirable for different applications. Helium-3 gas filled tubes have long been used as a standard for neutron detector due to their high neutron detection efficiency (~90% for thermal neutrons), low gamma sensitivity and large detection area (up to ~5 cm in diameter and ~200 cm in length) [1,2]. However, shortcomings such as poor portability, high bias voltage requirement (1200–1800 V), and high cost due to the limited supply of helium-3 (~$2000 per liter in 2011) [3] have resulted in increased research activities toward solid-state neutron detectors.

Since thermal neutron cross-sections of typical solid-state device materials such as Si, Ge and GaAs are low and interactions do not directly cause ionization, neutrons cannot be detected using only Schottky or p–n junction diodes. In order to overcome this issue, researchers have demonstrated planar solid-state neutron detectors with a layer of converter material coated on a semiconductor [4–6]. There are several converter materials available such as boron-10 (^{10}B), lithium-6 fluoride (^{6}LiF) and gadolinium-157 (^{157}Gd) for fabricating solid-state neutron detectors based on the ^{10}B(n,α)^{7}Li reaction, ^{6}Li(n,t)^{4}He reaction and ^{157}Gd(n,γ)^{158}Gd, respectively [7].

Of all the converter materials, ^{10}B is the preferred converter material by our group due to its high thermal neutron cross-section (~3840 barns) and its compatibility with Si processing technology [8]. When a thermal neutron interacts with ^{10}B, energetic charged particles, an alpha (α) particle and a lithium-7 (^{7}Li) ion, are produced. If these charged particles escape ^{10}B and reach Si, energy is deposited in the surrounding Si, creating electron–hole pairs. The interaction of neutrons with ^{10}B is summarized below [9].

$$ {}^{10}_{5}B + {}^{1}_{0}n \rightarrow \begin{cases} 6\%: & {}^{7}_{3}Li\ (1.015\ MeV) + {}^{4}_{2}\alpha\ (1.777\ MeV) \\ & Q = 2.792\ MeV\ \ (ground\ \ state) \\ 94\%: & {}^{7}_{3}Li^{*}\ (0.840\ MeV) + {}^{4}_{2}\alpha\ (1.470\ MeV) \\ & Q = 2.310\ MeV\ \ (1st\ \ excited\ \ state) \end{cases} $$

*: Corresponding authors.
E-mail addresses: huangk6@rpi.edu (K.-C. Huang), danony@rpi.edu (Y. Danon), bhati@rpi.edu (I.B. Bhat).

http://dx.doi.org/10.1016/j.nima.2014.06.047
0168-9002/

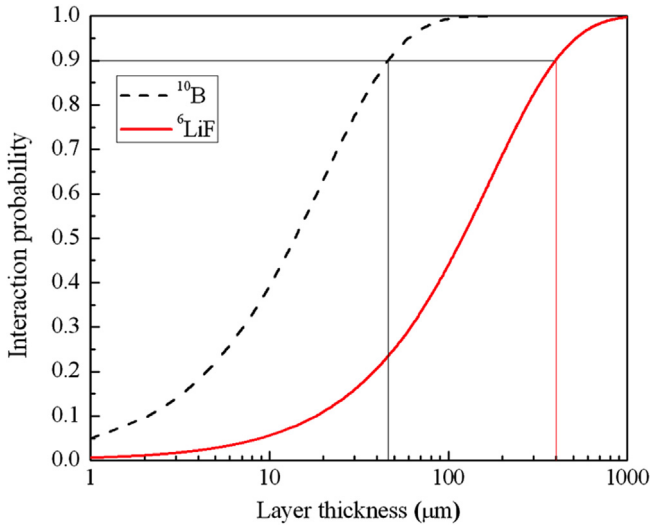

Fig. 1. Calculated thermal neutron (0.0253 eV) interaction probability as a function of ^{10}B and ^{6}LiF layer thickness.

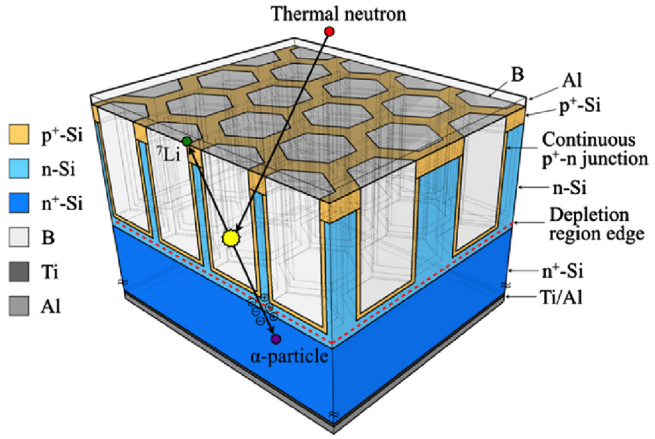

Fig. 2. Schematic of a three-dimensional honeycomb structured neutron detector and a basic working model (surface boron layer and boron etch stop layer are not shown in the schematic for clarity).

In order to maximize the neutron interaction probability, a ^{10}B layer (density ~2.35 g/cm^3) must be thick enough to interact with as many incident thermal neutrons as possible. Fig. 1 shows calculated thermal neutron (0.0253 eV) interaction probability as a function of ^{10}B and ^{6}LiF layer thickness. A ~45 μm thick ^{10}B layer results in a neutron interaction probability of 90%. However, the same neutron interaction probability in ^{6}LiF requires a layer thickness of ~400 μm. On the other hand, because the ranges of the α particles (1.47 MeV) and the ^{7}Li ions (0.84 MeV) in ^{10}B are ~2.8 μm and ~0.9 μm with an endpoint energy of 0.2 MeV, respectively, the ^{10}B layer must be thin enough (2–3 μm) to allow the generated charged particles to reach the p–n junction diode with sufficient energy to form a detectable number of electron–hole pairs. These conflicting requirements for the ^{10}B layer thickness limit the thermal neutron detection efficiency of planar detectors to 2–5% [10].

In order to overcome the limitation of the ^{10}B layer thickness for achieving higher neutron detection efficiency, researchers have proposed and demonstrated ^{6}LiF or ^{10}B filled micro-structured Si p–n diodes [7,11]. Our group proposed a ^{10}B filled high aspect ratio honeycomb structured solid-state neutron detector with a continuous p$^+$–n junction [12]. Fig. 2 shows a schematic of a three-dimensional honeycomb structured neutron detector and a basic working model for our proposed neutron detector. The basic configuration consists of a high aspect ratio, honeycomb structured Si p–n junction diode that is filled with ^{10}B. The ^{10}B is vertically thick enough to allow incident thermal neutrons to interact with the converter material and is also laterally thin enough to allow α particles and ^{7}Li ions to escape sideways. The initial portion of the boron filling process is used to form an *in situ* continuous p$^+$–n junction over the entire surface of the hexagonal holes so as to reduce the surface leakage current and deplete the Si wall completely.

In order to make solid-state neutron detectors competitive with the current ^{3}He-based neutron detection technology, which possesses a thermal neutron detection efficiency of up to 90% and a detection area of up to 5×200 cm^2, the neutron detection efficiency needs to be improved and the detection area also needs to be increased sufficiently. Bellinger et al. reported that an individual 4 cm^2 ^{6}LiF filled micro-structured neutron detector with a thermal neutron detection efficiency of 15.9% at −1 V can be improved to 29.0% by stacking two 4 cm^2 detectors back-to-back [13]. A stacked 36 cm^2 neutron detector was also fabricated, which exhibited a thermal neutron detection efficiency of 6.8% [14]. Previously, our group demonstrated a 2.5×2.5 mm^2 ^{10}B filled honeycomb structured neutron detector that can attain a thermal neutron detection efficiency of 26.1% at 0 V and a leakage current density of $\sim 2 \times 10^{-8}$ A/cm^2 at −1 V [15]. One of the main challenges associated with the scaling the detection area up is to keep the leakage current and the device capacitance low. Keeping these two parameters low will eliminate the need for segmentation of the detector and reduce the associated amplification electronics and will therefore reduce the overall cost of the system. Here, we report on the fabrication and characterization of such detector with an even lower leakage current density and a larger detection area (up to 16 cm^2) compared with our earlier published detector [15].

2. Experimental method

In order to fabricate 2.5×2.5 mm^2 neutron detectors as detector elements for a scalable large-area neutron detector, a 4-in. (1 0 0) oriented moderately doped n-Si wafer (resistivity ~0.5 Ω cm) was used as a substrate. A ~50 μm thick lightly doped n-Si layer (~50 Ω cm) and a ~1 μm thick heavily doped p-Si layer (~0.01 Ω cm) were epitaxially grown consecutively. 2.5×2.5 mm^2 device areas were isolated with mesa etching of the p-type epitaxial layer using photolithography and reactive ion etching (RIE) with sulfur hexafluoride (SF_6) and oxygen (O_2) plasmas. The exposed mesa sidewalls were then passivated with a ~1.5 μm thick silicon dioxide (SiO_2) layer. A ~300 nm thick SiO_2 layer was deposited in the device areas as a boron etch stop layer. High aspect ratio hexagonal holes were etched into the device areas using photolithography, dry etching of the boron etch stop layer and deep reactive ion etching (DRIE) of Si with a standard Bosch process [16]. In order to fabricate a continuous p$^+$–n junction over the entire surface of the hexagonal holes, a ~50 nm thick enriched boron layer (99.9% ^{10}B) was first deposited on the entire surface of the hexagonal holes at 510 °C for 5 min using a low-pressure chemical vapor deposition (LPCVD) system with a precursor of diluted enriched diborane (1% B_2H_6 in H_2). The ^{10}B layer was then diffused into the lightly doped n-Si in the same reactor at 800 °C for 10 min to form a continuous p$^+$-Si layer over the entire surface of the hexagonal holes. After forming the continuous p$^+$-Si layer, the hexagonal holes were completely filled with ^{10}B by LPCVD with the same precursor [17]. The ^{10}B on the contact areas was then selectively removed using photolithography and inductively coupled plasma reactive ion etching (ICP-RIE) with

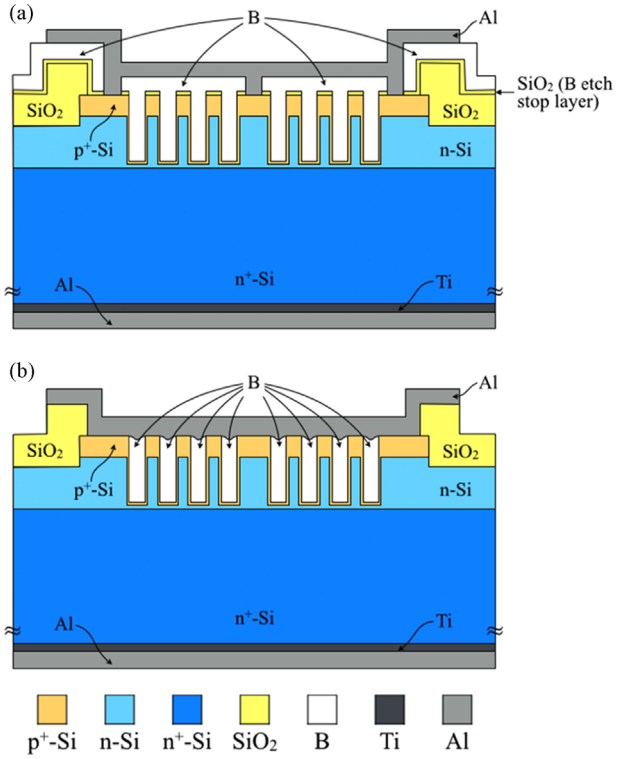

Fig. 3. (a) Cross-sectional schematic of our latest honeycomb structured neutron detector where ^{10}B is selectively removed from only the grid contact area, which leaves the ^{10}B in the device area intact, and (b) cross-sectional schematic of our previously reported honeycomb structured neutron detector where ^{10}B is entirely removed from the substrate surface using ICP-RIE followed by buffered oxide etching of a boron etch stop layer for metal contact.

SF_6/O_2 plasmas [17]. Finally, a ~1 μm thick aluminum (Al) with 2% Si was sputtered on the front side for p-contact and a 100 nm thick titanium (Ti) followed by a 900 nm thick Al were sputtered on the back side for n-contact. Fig. 3(a) shows a cross-sectional schematic of our latest detector where ^{10}B is selectively removed from only the metal grid contact area. In our previously reported detector, ^{10}B is entirely removed from the substrate surface using ICP-RIE followed by buffered oxide etching of the boron etch stop layer as shown in Fig. 3(b). During the ICP-RIE process, moderate over-etching of ^{10}B is required due to the non-uniformity in the surface ^{10}B layer thickness across the wafer. Therefore, not only does the surface ^{10}B get removed but the ^{10}B inside the holes and the thin p^+-Si layer on the vertical Si wall close to the hole opening may also get etched. This results in a decrease in the thermal neutron detection efficiency, an increase in the leakage current and can even short the device. The newer process for boron etching (Fig. 3(a)) is critical for reducing the leakage current further as shown in this paper.

After the metallization, the wafer was diced into 1 cm^2 individual dies with a standard semiconductor dicing saw for packaging. Each die contains fifteen 2.5×2.5 mm^2 sub-dies. The areas of the gaps between the 2.5×2.5 mm^2 sub-dies and the 1 cm^2 dies are not taken into account when scaling the detector area and calculating the efficiency. A 1 cm^2 individual die was mounted to a 24-pin gold socket package with silver paint as shown in Fig. 4(a). 2.5×2.5 mm^2 detectors in a 1 cm^2 die were individually wire bonded to the nearest pins in the gold socket package. With this testing module, the neutron detection efficiency of each 2.5×2.5 mm^2 detector can be measured separately. In order to measure the neutron detection efficiency of a 1 cm^2 detector, the p-contact metals of fifteen 2.5×2.5 mm^2 detectors were electrically shorted with silver paint, which was wire bonded as a single p-contact to the external pin for force connection as shown in Fig. 4(b). Fig. 4(c) shows an optical image of wire bonded 2.5×2.5 mm^2 detectors in a 24-pin gold socket package. Furthermore, in order to measure the thermal neutron detection efficiencies of detectors with detection areas larger than 1 cm^2, 1 cm^2 detector modules were connected in series by mounting individual modules in isolated zones on a copper (Cu) printed circuit board with silver paint. Cu wires were used as front-side connections to bond one detector to another in series. With a Cu printed circuit board, any number of detectors can be connected together to make a detector module with a desired detection area. Fig. 4(d) shows a schematic of a 4 cm^2 detector with four 1 cm^2 detectors connected in series on a Cu printed circuit board and Fig. 4(e) shows a schematic of an 8 cm^2 detector with two 4 cm^2 detectors connected in series. Fig. 4(f) shows an optical image of a 16 cm^2 detector with four 4 cm^2 detectors connected in series in an Al testing box. The intrinsic and relative thermal neutron detection efficiencies of 2.5×2.5 mm^2, 1 cm^2, 4 cm^2, 8 cm^2, 12 cm^2 and 16 cm^2 single-layer neutron detectors are shown and discussed in the next section.

3. Results and discussion

Fig. 5(a) shows a cross-sectional scanning electron microscope (SEM) image of ~45 μm deep and ~2.8 μm wide hexagonal holes separated by a ~1 μm thick Si wall fabricated using DRIE. The inset in Fig. 5(a) shows the top view SEM image of the hexagonal holes arranged in a honeycomb configuration. Fig. 5(b) shows simulated thermal neutron detection efficiency as a function of the hole diameter and wall thickness for a honeycomb configuration where the hole depth is fixed at 45 μm using a GEANT4 Monte Carlo toolkit [18,19]. The GEANT4 simulation considers the neutron flux as a parallel thermal neutron (0.0253 eV) beam normally incident on the detector surface and assumes the lower level discriminator (LLD) is 200 keV. From Fig. 5(b), it is clearly seen that the detection efficiency of the honeycomb configuration is much more sensitive to the wall thickness than the hole diameter. Therefore, the wall thickness has to be strictly controlled at ~1 μm to acquire the maximum efficiency (~48%).

The distinct feature of our work from previous work done by others is an *in situ* formation of a continuous p^+–n junction as a part of boron filling process by LPCVD over the entire surface of the Si substrate. Since the surface recombination from the etched Si wall is a major source of leakage current in such micro-structured diode, the fabricated continuous p^+–n junction is essential to significantly reduce the leakage current by reducing the surface recombination from the etched Si wall. Another distinguished feature is that the front-side ohmic contact metal only touches the thick p^+-Si region in the grid area. If the surface ^{10}B had been removed everywhere entirely, the thin p^+-Si layer on the vertical Si wall inside the hole may also get etched due to the over-etching of ^{10}B, which results in an increase in the leakage current and can short the device if the metal contact touches both the thick p^+-Si region and the n-Si substrate. As the leakage current contributes to the electronic noise, it reduces the ability of the neutron detector to detect small signals. Therefore, a neutron detector with an extremely low leakage current can achieve a good signal-to-noise ratio and a high neutron detection efficiency. Fig. 6 shows typical current density–voltage (J–V) characteristics of a 2.5×2.5 mm^2 honeycomb structured neutron detector with a continuous p^+–n junction. The curve with hollow squares shows a J–V curve under microscope light, and the curve with solid squares shows a J–V curve without illumination. The good photovoltaic characteristic of our detector with a fill factor greater than 75% ensures the performance of the diode and the capability of

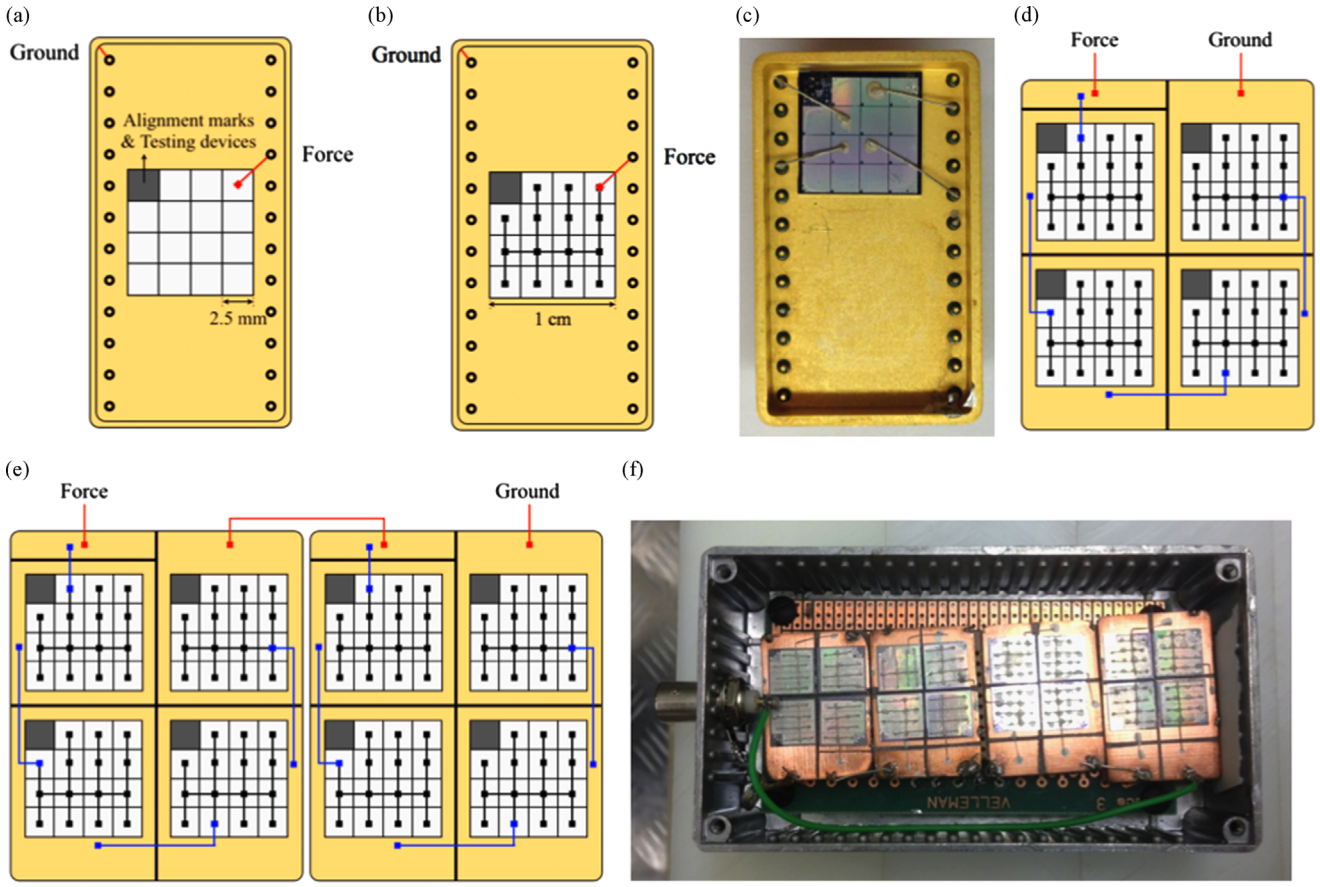

Fig. 4. (a) Schematic of a 2.5×2.5 mm^2 detector in a 24-pin gold socket package, (b) schematic of a 1 cm^2 detector with fifteen 2.5×2.5 mm^2 detectors connected in parallel in a 24-pin gold socket package, (c) optical image of wire bonded 2.5×2.5 mm^2 detectors in a 24-pin gold socket package, (d) schematic of a 4 cm^2 detector with four 1 cm^2 detectors connected in series on a Cu printed circuit board, (e) schematic of an 8 cm^2 detector with two 4 cm^2 detectors connected in series, and (f) optical image of a 16 cm^2 detector with four 4 cm^2 detectors connected in a series in an Al testing box.

operating the detector under self-biased condition (0 V). The leakage current density of the 2.5×2.5 mm^2 detector is $\sim 6.1 \times 10^{-9}$ A/cm^2 at -1 V, which is about 2 orders of magnitude lower than our previous result from a device fabricated without the introduction of the latest fabrication process of the front-side metal contact (Fig. 3(a)) [20]. This is the lowest leakage current compared to what we were able to find in the literature for such micro-structured Si diodes.

A californium-252 (^{252}Cf) neutron source, which emits fission neutrons moderated by a high-density polyethylene (HDPE) housing, was used to measure the intrinsic thermal neutron detection efficiencies of the detectors. The moderator housing has a volume of $61 \times 61 \times 40$ cm^3 with the ^{252}Cf source embedded in the center of the 61×61 cm^2 face, positioned 2.5 cm away from the side of the block. In order to accurately determine the average thermal neutron flux from the moderated source, the flux was measured at different distances using two methods: ^{6}Li-glass scintillator and gold foil activation. The average of the experimentally measured thermal neutron fluxes was compared with MCNP calculations and it was found that the measured values agree well with the MCNP simulations, giving an overall flux uncertainty of less than 5% [19,21]. The same MCNP simulation was also used to calculate the neutron flux spectrum as a function of energy incident on the face of the detector. This flux shape closely resembles a Maxwellian spectrum ($\varphi(E) \propto (E/KT)\exp(-E/KT)$), where the temperature (KT) is 0.034 eV, and was used to calculate the expected efficiency at the thermal point (0.0253 eV) from the measured Maxwellian averaged efficiency. The neutron flux at a distance of 10 cm from the front face of the moderator housing was 798 ± 40 neutrons/sec/cm^2 on the day of detector testing. In order to measure the efficiency, the detectors were placed in a lightproof Al testing box, connected to an ORTEC preamplifier (model: 142AH) [22] followed by an ORTEC shaping amplifier (model: 672). The pulse height spectrum of each detector was measured using an ORTEC MCA (model: 927) under self-biased condition (0 V). In order to obtain the intrinsic neutron detection efficiency, the counts were recorded by positioning the detector: (1) 10 cm away from the ^{252}Cf moderator face, (2) 10 cm away from the ^{252}Cf moderator face where the 61×61 cm^2 face was covered with a 2 mm thick Cd shield, (3) 5 cm away from a Cobalt-60 (^{60}Co) source (which provides an exposure rate of ~ 10 mR/h), and (4) with the ^{252}Cf source removed from the room for obtaining the electronic noise level. As the ^{252}Cf source in the moderator housing emits not only thermal neutrons but also fast neutrons and gamma rays, the Cd shield was used to shutter the neutrons with energy below 0.5 eV (thermal neutrons), allowing fast neutrons and gamma rays to pass. Since most nuclear materials emit about 10 or more times as many gamma rays as neutrons, a well-built neutron detector should have a high sensitivity to neutrons but a very low sensitivity to gamma ray interference ($\leq 10^{-5}$ at an exposure rate of 10 mR/h from a ^{60}Co source according to a report published by Pacific Northwest National Laboratory (PNNL) in 2009) [23]. Therefore, a LLD is set above the gamma response to avoid any contribution from the gamma rays to the intrinsic neutron detection efficiency. The gamma sensitivity of a neutron detector is defined here as the ratio of intrinsic gamma detection efficiency to intrinsic thermal neutron detection efficiency. In order to determine the energy endpoint of the pulse height spectrum, a GEANT4 simulation was performed on a 2.5×2.5 mm^2 detector with monoenergetic

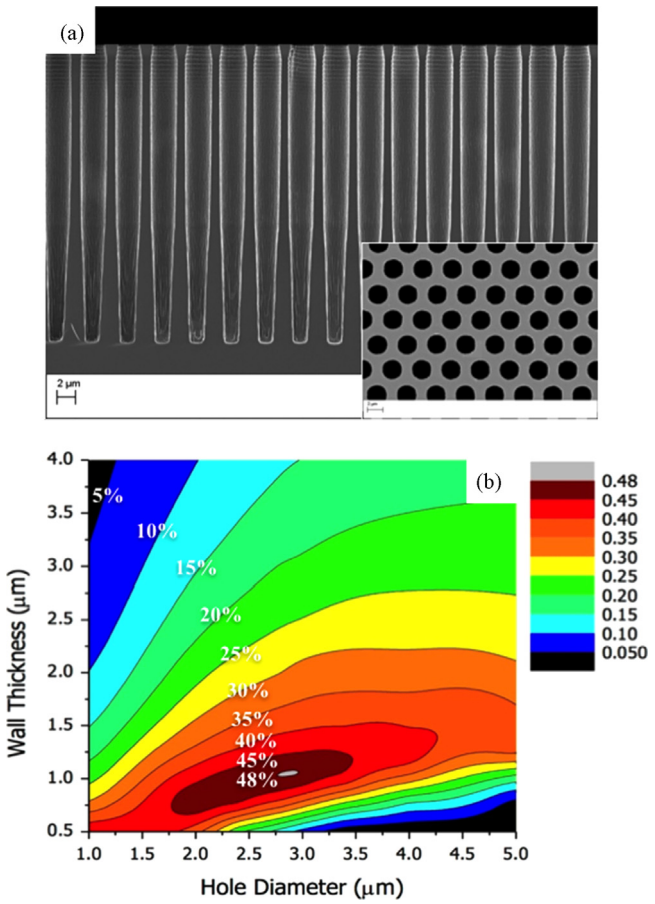

Fig. 5. (a) Cross-sectional SEM image of ~45 μm deep and ~2.8 μm wide hexagonal holes separated by a ~1 μm thick Si wall fabricated using DRIE. The inset in (a) shows the top view SEM image of the hexagonal holes arranged in a honeycomb configuration. (b) simulated thermal neutron detection efficiency as a function of hole diameter and wall thickness for a honeycomb configuration where the hole depth is fixed at 45 μm by using a GEANT4 Monte Carlo toolkit. The arrow in (b) indicates the direction of the increase in the simulated neutron detection efficiency.

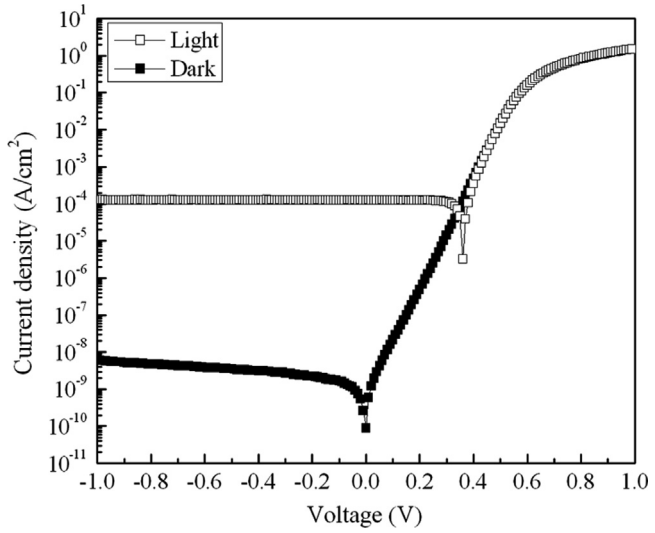

Fig. 6. *J–V* characteristics for a $2.5 \times 2.5\ mm^2$ honeycomb structured neutron detector with a continuous p^+–n junction. The curve with hollow squares shows a *J–V* curve under microscope light and the curve with solid squares shows a *J–V* curve without illumination.

neutrons (0.0253 eV) normally incident on the detector [19]. Fig. 7 compares the measured pulse height spectrum of a $2.5 \times 2.5\ mm^2$ detector under no external bias voltage with the GEANT4 simulation. The GEANT4 simulation fits the measured pulse height spectrum well, which verifies the device design and shows that the energy endpoint of the spectrum is ~2.5 MeV. Fig. 8 shows a measured pulse height spectrum of a $1\ cm^2$ detector under zero bias voltage with the *x*-axis normalized by assuming 2.5 MeV is the full charge particle energy deposition based on the GEANT4 simulation. The Maxwellian averaged thermal neutron detection efficiency of the best $1\ cm^2$ detector is $24.1 \pm 1.2\%$ under zero bias voltage with the LLD set to 370 keV. For the best $2.5 \times 2.5\ mm^2$ detector, with the LLD set to 400 keV, the Maxwellian averaged thermal neutron detection efficiency is $26.1 \pm 1.3\%$, and the gamma sensitivity is $(1.1 \pm 0.1) \times 10^{-5}$ under zero bias voltage [15]. The discrepancy between the measured neutron detection efficiency and the GEANT4 simulated neutron detection efficiency (~48%) could be related to hole profile and depth not being as designed

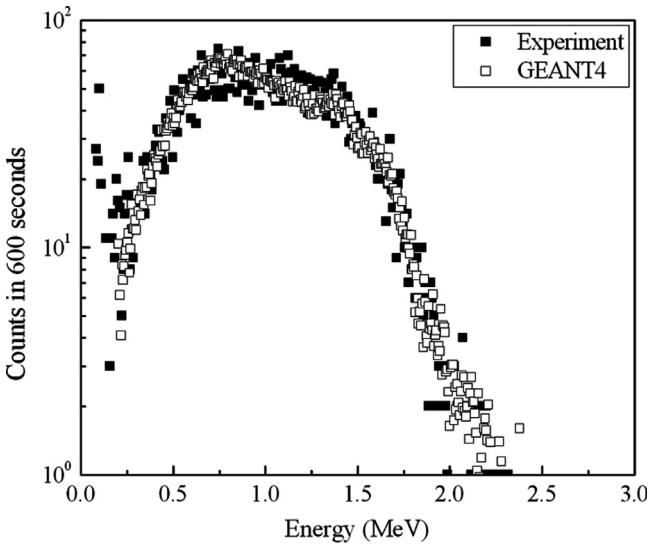

Fig. 7. Measured pulse height spectrum of a $2.5 \times 2.5\ mm^2$ ^{10}B filled honeycomb structured neutron detector under zero bias voltage and the GEANT4 simulation. The GEANT4 simulation well fits the measured pulse height spectrum, which verifies the device design and shows that the energy endpoint of the spectrum is ~2.5 MeV.

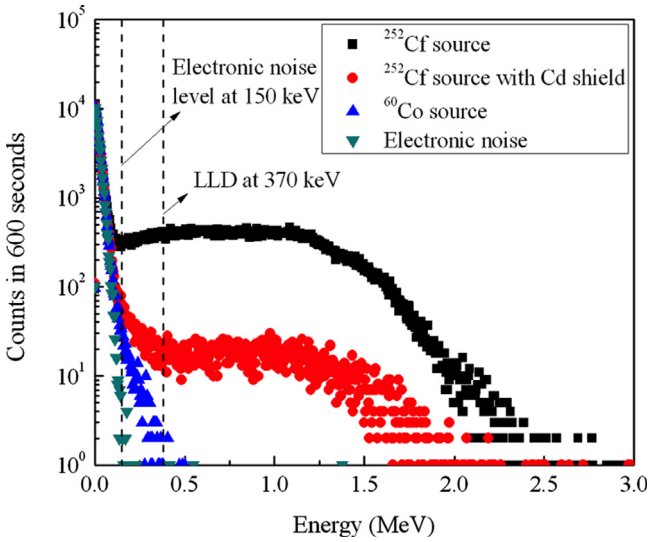

Fig. 8. Measured pulse height spectrum of a $1\ cm^2$ ^{10}B filled honeycomb structured neutron detector under zero bias voltage with the x-axis normalized by assuming the spectrum endpoint is the full charge particle energy deposition (~2.5 MeV) based on the GEANT4 simulation.

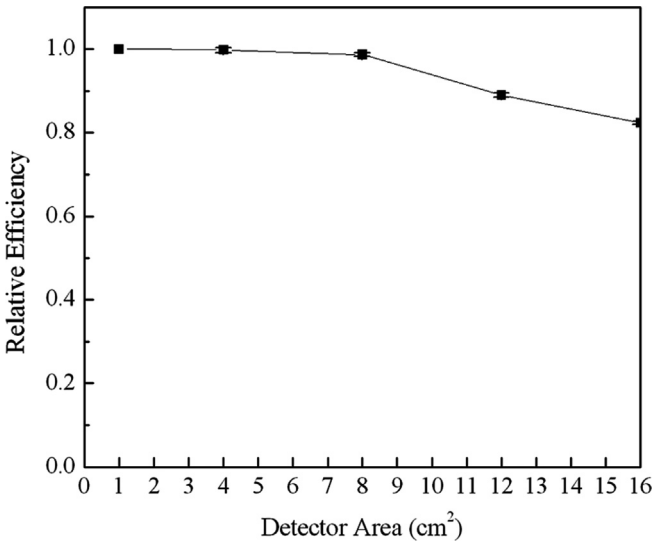

Fig. 9. Relative efficiency as a function of detector area.

(see Fig. 5(a)) and lower boron fill factor, which will be improved with a more optimized fabrication process.

The extremely low leakage current of our 2.5×2.5 mm^2 detector element (shown in Fig. 6) suggests that we can group these detector elements to realize and demonstrate the operation of a large-area neutron detector with a single pre-amplifier. In order to determine the maximum size of the detector that can be operated with a single pre-amplifier under the self-biased condition (0 V), single-layer neutron detectors with detection areas of 1, 4, 8, 12 and 16 cm^2 were assembled as shown in Fig. 4. The efficiencies of each 1 cm^2 detector unit that makes the large-area detectors were first measured individually and then measured in groups of 4, 8, 12 and 16 cm^2 in such a way that the positions of all the units were kept the same as when measured individually. Fig. 9 shows relative efficiency as a function of detector area. The relative efficiency is defined as the ratio of the count rate when measured in group to the sum of the count rates when measured individually. The reduction in the relative efficiency was not observed when scaling the detector area up to 8 cm^2 (the count rate when measured in group is about the same as the sum of the count rates when measured individually). However, the relative efficiency decreases to $\sim$0.89 and $\sim$0.82 for 12 and 16 cm^2, respectively. The 1 cm^2 detector units that make the large-area detectors were connected in series to ensure that the overall device capacitance remains low. In this configuration, the signal from one detector must pass through the others, and for large detector arrays it is expected that the signal-to-noise ratio will decrease as was observed. This result demonstrates the measurement capability of a scalable solid-state neutron detector up to 16 cm^2 without the need for segmentation, which requires additional amplification channels in order to maintain a high neutron detection efficiency.

4. Conclusions

In summary, scalable large-area single-layer thermal neutron detectors with detection areas up to 16 cm^2 were fabricated and demonstrated in this work by connecting individual 2.5×2.5 mm^2 detector elements externally. All of our large-area detector modules require only a single preamplifier, which is a major technological advancement in the field of solid-state neutron detection and shows the promise of using this technology for nuclear safeguard such as radiation portal monitors at security checkpoints. A reverse leakage current density of 6.1×10^{-9} A/cm^2 at -1 V for a 2.5×2.5 mm^2 detector is achieved, which is attributed to the formation of a continuous p^+–n junction over the entire honeycomb structured Si surface and the modified fabrication process of the front-side metal contact. With this low leakage current, a Maxwellian averaged thermal neutron detection efficiency of up to 26% and a gamma sensitivity of $\sim 10^{-5}$ for a 2.5×2.5 mm^2 detector element were measured under zero bias voltage. A thermal neutron detection efficiency of up to 24% was also measured for a 1 cm^2 detector module. Furthermore, no reduction in the relative efficiency was observed when scaling the detector area up to 8 cm^2. However, the relative efficiency decreases to 0.89 and 0.82 for 12 and 16 cm^2, respectively, when scaling the detector area beyond 8 cm^2. These results are promising for the emerging field of large-area solid-state neutron detector applications.

Acknowledgments

This work is supported by the U.S. Department of Energy - Nuclear Energy University Programs (NEUP) under award no. DE-AC07-05ID14517 and partially supported by the U.S. Department of Homeland Security - Domestic Nuclear Detection Office (DNDO) under award no. NSF/ECCS-1348269 and 2013-DN-077- ER0001. This support does not constitute an express or implied endorsement on the part of the Government.

References

[1] GAO (U.S. Government Accountability Office), Technology assessment: Neutron detectors: alternatives to using helium-3, GAO-11-753, 2011.
[2] J.F.C.A. Veloso, F. Amaro, J.M.F. dos Santos, J.A. Mir, G.E. Derbyshire, R. Stephenson, N.J. Rhodes, E.M. Schooneveld, IEEE Transactions on Nuclear Science NS51 (2004) 2104.
[3] D.A. Shea, D. Morgan, CRS Report for Congress 7–5700 (2010) R41419.
[4] A. Rose, Nuclear Instruments and Methods 52 (1967) 166.
[5] C. Petrillo, F. Sacchetti, O. Toker, N.J. Rhodes, Nuclear Instruments and Methods in Physics Research A 378 (1996) 541.
[6] D.S. McGregor, M.D. Hammig, Y.-H. Yang, H.K. Gersch, R.T. Klann, Nuclear Instruments and Methods in Physics Research A 500 (2002) 275.
[7] D.S. McGregor, W.J. McNeil, S.L. Bellinger, T.C. Unruh, J.K. Shultis, Nuclear Instruments and Methods in Physics Research A 608 (2009) 125.
[8] F. Sarubbi, T.L.M. Scholtes, L.K. Nanver, Journal of Electronic Materials 39 (2010) 162–173.
[9] G.F. Knoll, Radiation Detection and Measurement, Wiley, Hoboken, NJ, 2000.
[10] D.S. McGregor, R.T. Klann, H.K. Gersch, Y.-H. Yang, Nuclear Instruments and Methods in Physics Research A 466 (2001) 126.
[11] R.J. Nikolic, A.M. Conway, C.E. Reinhardt, R.T. Graff, T.F. Wang, N. Deo, C. L. Cheung, Applied Physics Letters 93 (2008) 133502.
[12] N. LiCausi, J. Dingley, Y. Danon, J.-Q. Lu, I.B. Bhat, Proceedings of SPIE 7079 (2008) 707908.
[13] S.L. Bellinger, R.G. Fronk, T.J. Sobering, D.S. McGregor, Proceedings of SPIE 8373 (2012) 83730I-1.
[14] S.L. Bellinger, R.G. Fronk, T.J. Sobering, D.S. McGregor, Applied Radiation and Isotopes 70 (2012) 1121.
[15] K.-C. Huang, R. Dahal, J.J.-Q. Lu, Y. Danon, I.B. Bhat, Applied Physics Letters 102 (2013) 152107.
[16] F. Laermer, A. Urban, R. Bosch, Milestone in deep reactive ion etch, in: Proceedings of the International Conference on Solid-State Sensors, Actuators and Microsystems, 2, 2005, p. 1118.
[17] K.-C. Huang, R. Dahal, J.J.-Q. Lu, Y. Danon, I.B. Bhat, Journal of Vacuum Science and Technology B 30 (2012) 051204.
[18] S. Agostinelli, J. Allison, K. Amako, J. Apostolakis, H. Araujo, P. Arce, M. Asai, D. Axen, S. Banerjee, G. Barrand, Nuclear Instruments and Methods in Physics Research Section A 506 (2003) 250.
[19] J. Clinton, Optimization and Characterization of a Novel Self Powered Solid State Neutron Detector (Ph.D. dissertation), Rensselaer Polytechnic Institute, Troy, NY, 2011.
[20] R. Dahal, K.-C. Huang, J. Clinton, N. Licausi, J.-Q. Lu, Y. Danon, I.B. Bhat, Applied Physics Letters 100 (2012) 243507.
[21] MCNP – A General Monte Carlo Code for Neutron and Photon Transport, Version 5, LA-UR-05-8617, Los Alamos National Laboratory, 2005.
[22] Ortec, 3630 Peachtree Rd, Atlanta, GA 30326, USA.
[23] R.T. Kouzes, J.H. Ely, A.T. Lintereur, D.L. Stephens, Neutron Detector Gamma Insensitivity Criteria, Pacific Northwest National Laboratory, Richland, WA, 2009.